# Fatigue damage and life evaluation of thick bi-material double strap joints for use in marine applications

Rahul Iyer Kumar[1] | Pankaj Jaiswal[1] | Wim De Waele[1]

[1]Ghent University, Department of Electromechanical, Systems and Metal Engineering, Soete Laboratory, Technologiepark-Zwijnaarde 46, 9052 Zwijnaarde, Belgium

**Correspondence**
Rahul Iyer Kumar
Ghent University, Department of Electromechanical, Systems and Metal Engineering
Soete Laboratory
Technologiepark-Zwijnaarde 46
9052 Zwijnaarde, Belgium
Email: Rahul.IyerKumar@UGent.be

The present-day interest in the use of composite-steel joints in primary marine applications requires an in-depth knowledge of the fatigue performance of thick adhesive joints. This paper reports on experimental tests, quasi-static and fatigue, performed on unaged and aged bi-material double strap joints with thick adhesive bondlines. The specimens are monitored by Digital Image Correlation and Infrared Thermography techniques to evaluate the types and extent of damage that occur in the joint during fatigue loading. The S-N curve of the aged joint is evaluated along with it's fatigue limit. It is found that the unaged specimens fail due to cohesive damage, hackles and disbond at the adhesive-adherend interface and the aged specimens failed due to delamination within the composite. The specimens that survived fatigue loading showed similar residual strength as specimens that were not fatigue loaded.

**KEYWORDS**
Marine, Offshore, Adhesive, Fatigue life, Damage evaluation, S-N curve, Residual strength

## 1 | INTRODUCTION

Modern marine vessels are traditionally built entirely from steel or are made of steel hull combined with an aluminium superstructure. One of the advantages of using metals is that the joints in the vessel can be easily designed and

realised by welding and riveting[1]. Composite materials are considered as an alternative to metals, especially in the ship superstructure, where replacing parts or even the entire superstructure significantly reduces the overall weight resulting in increased stability of large ships and reduced fuel consumption. This increases the need for robust and well-controlled techniques for realising bi-material joints. Mechanical fasteners such as rivets, bolts and screws have dominated joining techniques for multi-material components, due to the cheap component cost and relatively easy assembly and disassembly processes. However, for composite materials, the application of mechanical fasteners would be counterproductive. Fibre reinforced polymers (FRP's) are weak in the direction normal to the fibre direction, where the strength is dominated by the polymer matrix which restricts the amount of pretension that can be applied to the fasteners and therefore limits the contact pressure between the two joint faces. Besides, a hole through the composite plate introduces a discontinuity of the fibres, decreasing its desired strength properties. For these reasons, the use of adhesives to join the composite superstructure with the steel hull makes logical sense. The use of adhesive joints is already widespread in the aerospace and automotive industry, but not so in the shipbuilding industry[2]. This is due to the fact that in aerospace applications very thin layers of adhesives are used and extensive pre-treatment of surfaces is employed which do not comply with tolerances and manufacturing practices used in the shipbuilding and offshore industry. In addition, the bonded structure must be able to operate safely and reliably for a long-term in the order of 20 to 25 years or longer in a marine environment. It is therefore crucial to provide the marine and offshore industry with engineering data that can be used for predicting the life expectancy and structural integrity of the adhesively bonded components[3].

The current work is divided into two parts. The first part deals with evaluating bi-material thick adhesive joints to gain insight into the various damage mechanisms and their evolution under fatigue loading. The second part deals with evaluating the fatigue life of thick adhesive joints which are aged in a salt-spray chamber to mimic the interface degradation which occurs in the harsh marine environment. Following a concise literature review, the specimen configurations and test methods are discussed. The adhesive joint is subjected to quasi-static tensile tests, constant amplitude fatigue tests, block loading fatigue tests and spectrum loading to quantify various aspects of the joint fatigue properties and the relevant damage mechanisms. Fatigue damage evolution is monitored using Digital Image Correlation (DIC) and Infrared Thermography (IRT). Next, the results from the various fatigue experiments are presented along with DIC and IRT analysis. Additionally, a quasi-static tensile test is performed on samples that survived the fatigue loading to determine their residual strength. Finally, a summary and the main conclusions of this research are provided.

## 2 | LITERATURE REVIEW

Tests performed on adhesives are mainly categorized into two main approaches. The first is to determine basic physical and mechanical properties to support the selection of adhesives, and is mainly performed on bulk adhesive specimens. The second approach aids the design process by assessing the quality of the bonded joint, which is refereed to as in-situ testing[3]. Reported fatigue studies on adhesive joints have focused primarily on components made of single adherend material such as metal-to-metal or composite-to-composite and joints with relatively thin bondline thicknesses. Harris and Fay[4] evaluated the fatigue life and the failure mechanisms of single lap joints made of mild steel typically used in exterior automotive panels, at different temperatures with two types (toughened epoxy and polybutadiene) of structural adhesives, and two different bondline thicknesses of 0.2 mm and 2 mm. They concluded that the fatigue resistance is hindered at temperatures above the glass transition temperature ($T_g$) and that thinner bondlines show longer fatigue life at all temperatures. For thicker bondlines, they showed that the crack initiated

more frequently at diagonally opposite interfaces near the joint edges and propagated towards each other leading to failure at the centre of the joint. Banea and da Silva [5] state that, once a crack propagates in an adhesively bonded joint, the geometrical and loading symmetries are immediately lost which in-turn lead to local bending stresses. Such stress state in a joint where a composite is the adherend, could lead to premature failure of the composite before failure in the adhesive. Composite failure is predominantly inter-laminar delamination near the surface of the composite adherend [6]. It was further shown that the delamination is prevalent in joints with quasi-isotropic composite and cohesive failure in unidirectional composite joints [7].

A lot of research has been done to study the differences in static strength of adhesive joints with thin and thick bondline thicknesses. It is concluded that the strength of the lap joint decreases with increase in bondline thickness [8]. It is hypothesised that this difference in strength is due to the *plastic spreading* of the adhesive; in other words, the stresses are more uniformly distributed in the thicker bondline when compared to the thin bondlines where the stresses are more concentrated near the ends of the overlap [9]. Finite element analysis based on the stresses at the interface between adhesive and adherend as failure criterion showed that the peel and shear interface stresses are higher for thicker bondlines [10]. Assuming that final failure occurs in the vicinity of the adhesive-adherend interface, this theory explains why thinner bondlines are stronger than thicker ones. An older and more straightforward theory by Adams and Peppiatt argues that thick adhesive bondlines inherently contain more defects like micro cracks and voids, leading to lower strengths [11].

Fatigue data is generally represented in the form of an $L - N$ or $S - N$ curve, which plots the number of cycles ($N$) required to cause failure in a specimen against the applied load ($L$) or average stress value ($S$). The properties of a bonded joint subjected to fatigue is a function of adhesive and adherend material properties, the loading type, and the joint geometry. It is hence necessary to perform cyclic tests on representative joints similar to those to be used in service [3]. Fatigue tests have been performed on metal-to-metal single lap joint test specimens with bondline thickness of 0.1mm to 2mm [4;12;13], metal-to-metal double strap joints with bondline thickness of 0.13mm [14], composite-to-composite double lap joints with bondline thickness of 0.2mm and 2mm [15-18], composite-to-metal double strap joints with bondline thickness of 0.5mm and 2mm [19-22]. Additionally, the effect of environmental conditions along with fatigue loading on composite-to-metal double strap joints with thin bondline thickness was studied by *Borrie et al.* and *Yu et al.* [21;23], who concluded that the harsh environmental conditions and fatigue are detrimental to the bond strength and stiffness of the joints.

As discussed above, numerous studies have been carried out to determine the fatigue properties of bonded joints with various joint configurations and different adherend materials under harsh environmental conditions. Most of them address the fatigue properties of joints with brittle epoxy adhesives and a bondline thickness from few microns to a maximum of 2 to 3mm. With respect to composite-to-metal joints, the focus is on using composites to repair the structural or marine components in order to extend their service life. To the best of the authors' knowledge, very limited research has been done on specimens with ductile and tough adhesive and bondline thickness in the millimetre range which are relevant to marine and offshore industries where tolerances less than the millimeter range are hard to achieve in a shipyard.

# 3 | MATERIALS AND METHODS

## 3.1 | Joint configuration

Tests were performed on double strap joint specimens manufactured by Damen Naval. The bi-material joints were made from 8mm thick flat steel bars (grade AH36) and 3mm thick CFRP laminates bonded together with a two-
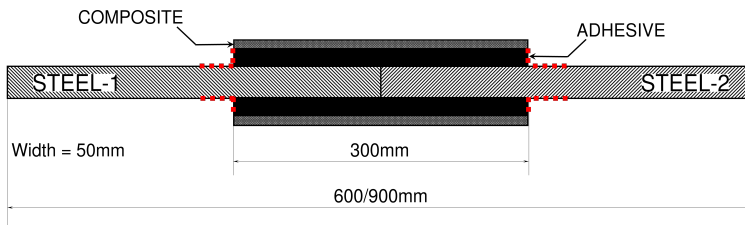
**FIGURE 1** Schematic representation of the bi-material thick adhesive joint. Red dotted lines indicating the region which is left uncoated by anti-corrosive paint

component methyl-methacrylate (MMA) adhesive with a nominal bondline thickness of 4mm or 8mm and an overlap length of 300mm as shown in Figure 1. The specimens were manufactured by bonding large steel plates and composites panels with the desired adhesive bondline thickness and later sectioned to a width of 50mm using water jet cutting. Ten specimens of bondline thickness 4mm and 8mm and a total length of 900mm were tested in the as-received condition (*unaged*). Additionally, a total of 18 specimens were subjected to salt-spray exposure (*aged*); these specimens had a total length of 600mm and bondline thickness of 8mm. Before the aged samples were water jet cut to the desired width, they were coated with anti-corrosive paint to protect the steel and composite surfaces. A small region at the interface of steel and adhesive was left uncoated (red dotted lines in Figure 1) in order to artificially accelerate the ageing process at the interface. The ageing of the samples was done by placing the large coated panels in a salt-spray chamber for a period of 6 weeks, where the conditions for ageing were set according to ASTM B117-11 standard [24], i.e., 5% salinity, 35°C and 50% humidity. The unaged specimens are predominantly used as reference and to assess the various damage mechanisms during fatigue, whereas the aged specimens are used to determine the fatigue properties of the bi-material bonded joint in terms of an S-N curve.

## 3.2 | Testing procedure

Quasi-static tensile tests were performed on a servo-hydraulic machine with a load cell of capacity 1000kN and the fatigue tests were performed on machines with a load cell capacity of 100kN and 150kN. A schematic representation of the test setup is shown in Figure 2. During each test, besides recording the load and actuator displacement, DIC and IRT are used to monitor the evolution of deformation and temperature in the specimen respectively.

DIC is a contactless optical technique that makes use of a speckle pattern applied to the specimen's surface to measure the deformations and strains at the surface [25]. The system consists of two cameras having a 9 megapixel sensor ($4112 \times 2176$ pixels), that are placed at an angle to the specimen. Images are captured from both the cameras simultaneously during testing and VIC-3D software from Correlated Solutions is used for the post-processing of the captured images to determine the deformations and strains on the surface of the specimen. ImageIR 8300 camera along with IRBIS3 software from InfraTec GmbH is used to capture and post-process thermal data from the specimen during fatigue experiments. The infrared camera captures data in the infrared spectral range of $2-5.7\mu m$, with a sensor of size $640 \times 512$ IR pixels. The camera is equipped with a sterling cooler which increases the sensitivity and accuracy of the thermal images. The camera can measure temperature in the range of $-40°C$ to $1500°C$ with a resolution of $20mK$ at 30°C. One of the challenges of using the IRT technique to determine the temperature of a specimen during testing is that the specimen surface should have uniform emissivity i.e., avoiding reflective surfaces. To mitigate this problem, the specimen to be tested is painted black with a matt finish.

After the experiment, fractographic images of ruptured specimens are taken with the help of a digital camera. This
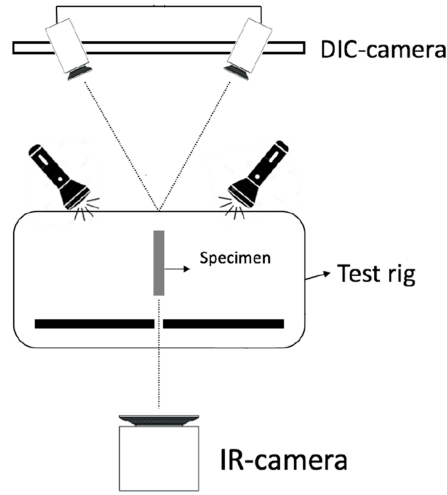
**FIGURE 2** Schematic representation of the test setup

approach allows to avoid falsely identifying failure modes which may arise when high-resolution imaging techniques (eg. SEM) are used to study the failure surface of the joint post-mortem[26].

### 3.2.1 | Quasi-static tensile test

A quasi-static tensile test was performed to quantify the tensile strength of specimens with different bondline thickness and ageing condition. This load and in turn the corresponding maximum value of the average shear stress in the adhesive was used in determining the appropriate load/stress levels to be applied during fatigue tests. The quasi-static tensile tests were performed at a displacement rate of 0.5mm/min. The average shear stress ($\tau_{avg}$) and shear strain ($\gamma_{avg}$) which are assumed to be uniform over the thickness are calculated according the equations (1) and (2) respectively, where $P$ is the force in N, $w$ the specimen width in mm, $2l$ the total overlap length in mm, $d$ the elongation of the specimen in mm and $t$ the adhesive bondline thickness in mm.

$$\tau_{avg} = \frac{P}{2wl} \tag{1}$$

$$\gamma_{avg} = \frac{d}{2t} \tag{2}$$

### 3.2.2 | Fatigue test

The fatigue tests are conducted by controlling the force that is applied to the double strap joint. The force applied to the specimen is in the form of a sinusoidal wave with load ratio R=0.1 and a frequency of 4Hz. DIC and IRT cameras are triggered to take snapshots of the state of deformation and temperature respectively of the specimen at regular intervals during the test. Three different types of fatigue loading were applied to the test specimens; (i) a constant amplitude fatigue (CAF) load, where the specimens were subjected to constant load amplitude until complete failure or

until a pre-defined run-out of five million cycles, (ii) a block loading fatigue (BLF), where the specimens were subjected to sequences of constant load amplitude for a predefined number of cycles (blocks) after which the load amplitude is increased until the specimen fails, (iii) spectrum loading (SL), where the specimens were subjected to particular load amplitudes (in decreasing order) for predefined numbers of cycles. The basis for selecting the loads for the spectrum loading is explained section 4.2.2.

### 3.2.3 | Residual tensile test

The aged specimens which survived the predetermined number of cycles during the fatigue tests without rupturing, were tested quasi-statically to determine their residual strength. The test was performed at a displacement rate of 0.5mm/min, similar to that chosen in the quasi-static tensile test.

### 3.2.4 | Statistical testing

A hypothesis test (Welch's t-test) is employed to determine if there is any difference between the shear strength of specimens that were subjected to quasi-static tensile testing and the residual tensile tested specimens. The null hypothesis is that the mean shear strength of the two groups are equal ($H_0 : \mu_{quasi\text{-}static} = \mu_{residual}$) and the alternate hypothesis is that the mean values of the two groups are different ($H_1 : \mu_{quasi\text{-}static} \neq \mu_{residual}$) with a significance level of $\alpha = 0.05$.

### 3.3 | Analysis of DIC and IRT images

DIC images are used during quasi-static tensile testing primarily to determine the extension of the specimen with the help of a virtual extensometer. Besides, it allows to determine the onset of various damage mechanisms such as hackles in the adhesive and disbond at the adhesive-adherend interface. The IRT images captured during the test allow to analyse the temperature evolution along the entire length of the specimen during a fatigue test by slicing the image area into multiple regions as shown in Figure 3. A reference temperature (R94 indication on the figure) is also recorded using a sample of the same adhesive kept in the frame of the infrared camera. This reference temperature allows to determine the load and damage related temperature changes in the double strap joint by subtracting the environmental temperature change. With this information, it is possible to visualise and analyse the temperature evolution of the double strap joint both in time and along it's length.

## 4 | RESULTS AND DISCUSSIONS

### 4.1 | Quasi-static tensile test

The quasi-static tensile test results for the unaged and aged double strap joint specimens are shown in Figure 4a and Figure 4b respectively. The main strength properties are summarised in Table 1a and Table 1b. Analysing the fractography images of the ruptured specimens, it was observed that four out of five specimens failed due to delamination within the CFRP laminate. Specimen 10 failed due to a combination of cohesive failure in the adhesive and delamination of the composite layers in the CFRP laminates as seen in Figure 5. The aged double strap joints showed a mean $\tau_{avg_{max}}$ of 6.91 MPa with a standard deviation of 0.41 MPa.
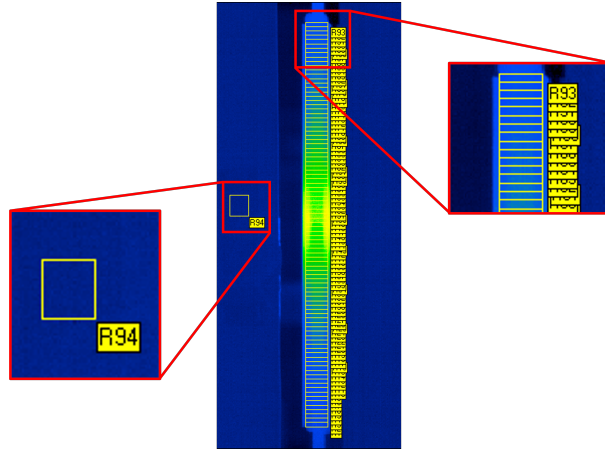
**FIGURE 3** Typical IRT image showing the double strap joint specimen spliced into multiple regions along its length (R1 – R93) and the reference temperature region (R94)

## 4.2 | Fatigue testing

### 4.2.1 | Unaged specimens

A total of eight unaged double strap joints were subjected to various fatigue load schemes as described in section 3.2.2. A brief summary of the different loads and the number of cycles the specimen was able to withstand before failure or otherwise is given in Table 2a. Due to the long experimentation time in fatigue testing, the specimens were tested to a maximum of $5 \times 10^6$ cycles. Any specimen that survives this threshold is referred to as *runout* specimen. As the experiments on unaged samples were done primarily to study the damage mechanisms, some specimens were tested for more than $5 \times 10^6$ cycles.

**Constant amplitude fatigue**

Specimens 1 and 2 with 4mm bondline thickness were CAF loaded with maximum average shear stress ($\tau_{avg_{max}}$) of 2.0 MPa and 2.5 MPa respectively. Both specimens remained intact after the $5 \times 10^6$ cycle mark and showed no signs of damage. Specimen 1 was tested for $5.14 \times 10^6$ cycles and specimen 2 for $5.78 \times 10^6$ cycles before the experiment was stopped. The tests were carried out beyond the runout number of cycles to evaluate the possibility of failure shortly following this artificial cycle mark. Analysing the raw and post-processed DIC images in Figure 6a it can be seen that no indications of damage (eg. hackles, cracks, disbonds) occur after $4.75 \times 10^6$ cycles, this remained the case even after the testing.

Specimen 3 and 4 with 8mm bondline thickness were also loaded under CAF. Specimen 3 was tested for $2.72 \times 10^6$ cycles before the experiment was stopped. The specimen was not completely ruptured but showed signs of severe damage. Specimen 4, on the other hand, failed after $3.58 \times 10^6$ cycles. Analysing the raw and post-processed DIC images of specimen 3 in Figure 6b, it is evident that there is damage in the bulk adhesive in the form of cracks which inclined at an angle of 45°, known as hackles (indicated by yellow circles), which occur when the adhesive is loaded beyond its elastic capability[27]. It can also be observed that disbond occurs at the adhesive-composite interface near the centre of the specimen (indicated by red circles). The region around these damages shows a lower strain in comparison with the neighbouring regions, as seen in the post-processed DIC image. Similarly, specimen 4
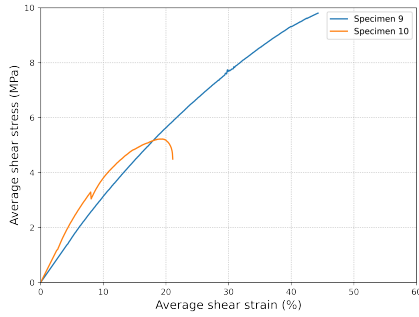
(a) Unaged specimens
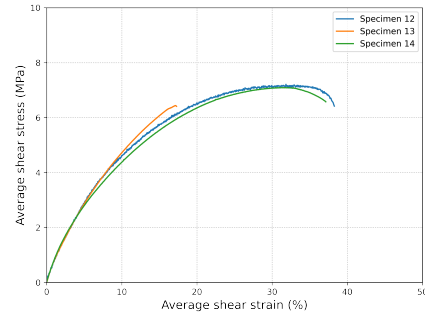


(b) Aged specimens

**FIGURE 4** Average shear stress versus average shear strain curve for quasi-static tensile tests on unaged and aged double strap joints

**TABLE 1** Summary of the results from the quasi-static tensile tests

(a) Unaged specimen

| Specimen no. | Max. load | $\tau_{avgmax}$ | Elongation at failure | $\gamma_{avgmax}$ |
|---|---|---|---|---|
| 9 | 147.01 kN | 9.80 MPa | 3.50 mm | 43.75% |
| 10 | 78.30 kN | 5.22 MPa | 3.40 mm | 21.25% |

(b) Aged specimen

| Specimen no. | Max. load | $\tau_{avgmax}$ | Elongation at failure | $\gamma_{avgmax}$ |
|---|---|---|---|---|
| 12 | 108.16 kN | 7.21 MPa | 6.12 mm | 38.25% |
| 13 | 96.58 kN | 6.44 MPa | 2.77 mm | 17.31% |
| 14 | 106.40 kN | 7.09 MPa | 5.94 mm | 37.13% |

also developed hackles in the adhesive during fatigue; in addition to the previously described disbond at the adhesive-composite interface, disbonds also occurred near the top of the specimen at the steel-adhesive interface. This disbond at the steel-adhesive interface grew rapidly and due to asymmetry induced a bending moment in the joint leading to rupture of the specimen.

## Block loading fatigue

The 4mm bondline specimens 5 and 6 were subjected to block loading fatigue with blocks of $100,000$ cycles and $50,000$ cycles respectively. Specimen 5 ruptured after $8.23 \times 10^5$ cycles and specimen 6 ruptured after $4.27 \times 10^5$ cycles with $\tau_{avgmax} = 4.5$ MPa at failure for both specimens. Specimens 7 and 8 with bondline thickness of 8mm were subjected to blocks of 100,000 cycles and 50,000 cycles respectively. Specimen 7 ruptured after $6.62 \times 10^5$ cycles with $\tau_{avgmax} = 3.5$ MPa at failure and specimen 8 ruptured after $2.66 \times 10^5$ cycles with $\tau_{avgmax} = 3.0$ MPa at failure. All specimens subjected to BLF failed predominantly due to cohesive failure within the adhesive in addition
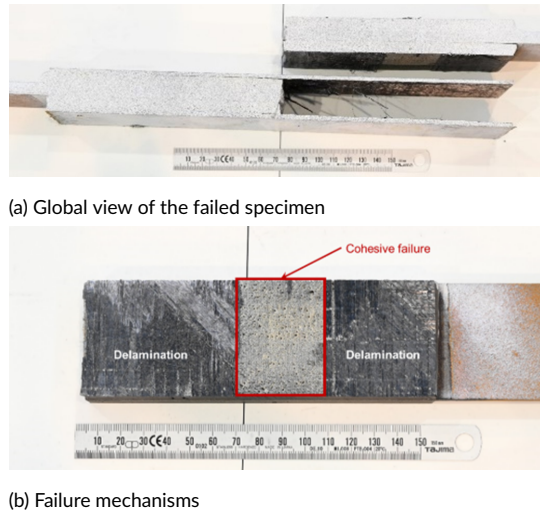
(a) Global view of the failed specimen



(b) Failure mechanisms

**FIGURE 5** Fractography images of specimen 10. (a) Global view of the failed specimen; (b) Delamination in the CFRP composite layer and cohesive failure of the adhesive which leads to the failure of the specimen.
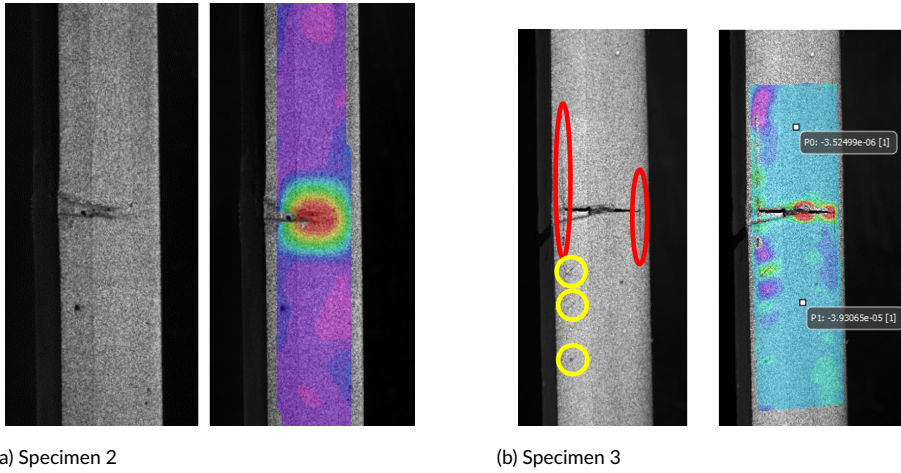


(a) Specimen 2



(b) Specimen 3

**FIGURE 6** **(a)** State of specimen 2 after after $4.75 \times 10^6$ cycles shows no signs of damage in the raw DIC and post-processed images **(b)** Raw DIC and post-processed images of specimen 3 after $1.60 \times 10^6$ cycles with damage types indicated on the left. Red ellipses: disbond at the adhesive-composite interface; yellow circles: hackles

to showing disbond at the steel-adhesive interface. On closer inspection of the 4mm bondline specimens, ridge like formations are found on the cohesive damage surface as shown in Figure 7. The 8mm bondline specimens show this to a lesser extent. This surface state is due to the absolute temperature in the specimen reaching a value close to the glass transition temperature of the adhesive due to self-heating at high cyclic stress.

**TABLE 2** Summary of fatigue test results

(a) Unaged specimens - 4mm and 8mm bondline thickness

| Specimen no. | Loading type | Remarks on fatigue loading | Total number of cycles | State of specimen |
|---|---|---|---|---|
| 1 (4 mm) | CAF | $\tau_{\text{avgmax}}$ = 2.0 MPa | $> 5.00 \times 10^6$ | Intact |
| 2 (4 mm) | CAF | $\tau_{\text{avgmax}}$ = 2.5 MPa | $> 5.00 \times 10^6$ | Intact |
| 5 (4 mm) | BLF | steps of 0.5 MPa | $8.23 \times 10^5$ | Failed |
| 6 (4 mm) | BLF | steps of 0.5 MPa | $4.27 \times 10^5$ | Failed |
| 3 (8 mm) | CAF | $\tau_{\text{avgmax}}$ = 2.0 MPa | $2.72 \times 10^6$ | Intact(*) |
| 4 (8 mm) | CAF | $\tau_{\text{avgmax}}$ = 2.5 MPa | $3.58 \times 10^6$ | Failed |
| 7 (8 mm) | BLF | steps of 0.5 MPa | $6.62 \times 10^5$ | Failed |
| 8 (8 mm) | BLF | steps of 0.5 MPa | $2.66 \times 10^5$ | Failed |

(b) Aged specimens - 8mm bondline thickness

| Specimen no. | Loading type | Remarks on fatigue loading | Total number of cycles | State of specimen |
|---|---|---|---|---|
| 16 | CAF | $\tau_{\text{avgmax}}$ = 6.0 MPa | 1,520 | Failed |
| 17 & 24 | CAF | $\tau_{\text{avgmax}}$ = 4.0 MPa | 12,606 & 6,375 | Failed & Failed |
| 19 & 25 | CAF | $\tau_{\text{avgmax}}$ = 3.0 MPa | 87,000 & 68,946 | Failed & Failed |
| 21 & 22 | CAF | $\tau_{\text{avgmax}}$ = 2.5 MPa | $5.00 \times 10^6$ & $2.25 \times 10^6$ | Runout & Failed |
| 18 & 26 | CAF | $\tau_{\text{avgmax}}$ = 2.0 MPa | $5.00 \times 10^6$ & $5.00 \times 10^6$ | Runout & Runout |
| 20 & 23 | CAF | $\tau_{\text{avgmax}}$ = 1.0 MPa | $5.00 \times 10^6$ & $5.00 \times 10^6$ | Runout & Runout |
| 27 | BLF | Blocks of 150,000 cycle | 909,141 | Failed |
| 28 | BLF | Blocks of 100,000 cycle | 639,171 | Failed |
| 29 & 30 | SL | | $3.47 \times 10^6$ & $3.47 \times 10^6$ | Runout & Runout |

(*): testing stopped before rupture and before $5 \times 10^6$

CAF: Constant amplitude fatigue; BLF: Block loading fatigue; SL: Spectrum loading

The specimen numbers do not indicate the order in which they were tested

**Temperature evolution**

The general trend of the temperature evolution is elucidated by analysing one specimen subjected to CAF and one specimen subjected to BLF. In each case, the relative and normalised temperature evolution in the specimen were analysed. Relative temperature refers to the temperature of all regions along the length of the specimen minus the reference temperature (R94, see higher). The normalised temperature, on the other hand, refers to the ratio of the temperature intensity of all regions along the length of the specimen and the maximum temperature in the specimen.

The evolution of temperature in specimen 2 subjected to CAF and specimen 7 subjected to BLF is shown in Figure 8a and 8b respectively. For specimen 2, it should be noted that not the entire specimen length has been monitored. The thermal camera was primarily focused on the top part of the specimen to obtain a better image resolution. Initially, the temperature in the specimen is rather uniform. As the fatigue cycles accumulate, the temperature concentrates near the centre of the specimen at the discontinuity between the two steel bars. The maximum normalised
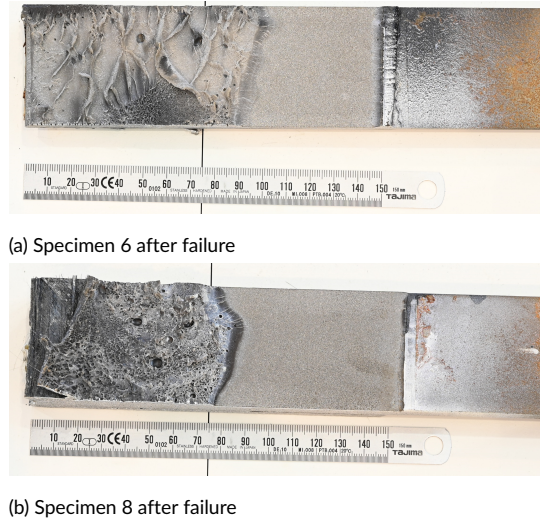
(a) Specimen 6 after failure



(b) Specimen 8 after failure

**FIGURE 7** Fractography image of specimens 6 and 8 showing ridge like formations on the cohesive damage surface

temperature (value 1) is more or less situated around the 150mm mark, i.e. the centre of the specimen. Contrary to the analysis of the CAF temperature data, it can now be observed that the location of the maximum temperature changes during the BLF. Initially, it is similar to the CAF and occurs near the centre of the specimen. As the fatigue test progresses and the load applied on the specimen is sequentially increased, it can be observed that two hot spots occur in the specimen after 200,000 cycles. In the sixth sequential block, the region of maximum temperature starts to increase in size and once the last sequential block starts, it rapidly moves upwards along the specimen, leading to rupture. Comparing the maximum temperature location data with the fractography images of the specimen shown in Figure 8c, it is clear that the maximum temperature corresponds to the cohesive type of damage in the adhesive denoted by the red boxes. The temperature increase at the region of cohesive damage may be due to internal friction between cracked adhesive surfaces. Delamination of composites and disbond between interfaces is not captured by the IRT data. It is hypothesised that these damages occurred without significant heat dissipation and that they are overshadowed by the temperature signals from the cohesive damage.

## 4.2.2 | Aged specimens

A total of fifteen aged double strap joints were subjected to various fatigue load schemes as described in section 3.2.2. A brief summary of the different loading levels and the number of cycles the specimen was able to withstand before failure or otherwise is given in Table 2b.

**S-N curve**

The S-N curve based on the constant amplitude fatigue experiments is shown in Figure 9. The fatigue limit for the aged bi-material double strap joint is defined as 1.0 MPa. At this stress level the specimen showed no signs of damage, neither disbond at the adhesive-adherend interface nor hackles in the adhesive. The S-N curve can be represented as $N = a \cdot S^{-m}$, with $a = 15.81$ and $m = 0.14$. At an average shear stress level of 2.0 MPa, the tested specimens did not
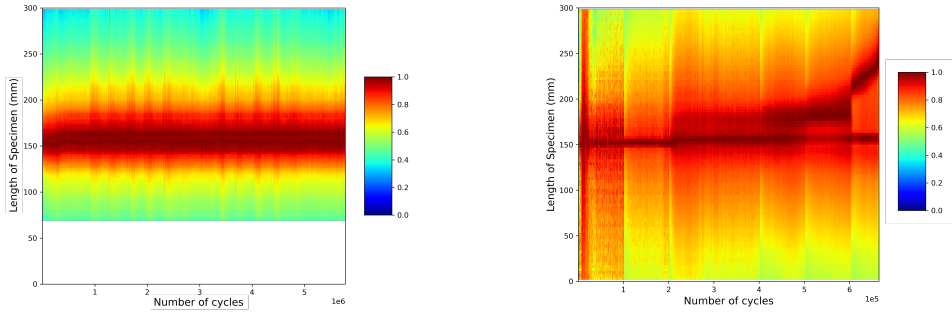
(a) Temperature evolution during CAF



(b) Temperature evolution during BLF
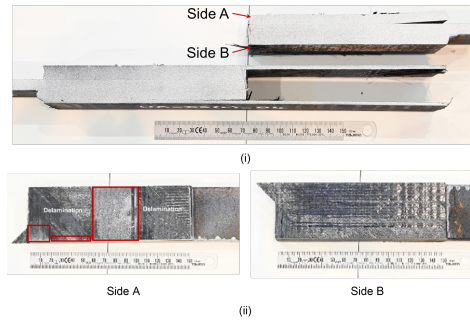


(c) Fractography image of specimen 7

**FIGURE 8**    (a) and (b) Evolution of temperature in specimens 4 and 7 during CAF and BLF tests captured using IRT camera. (c) Fractography images: (i) after rupture (ii) and a closer view of the two sides of the top half of the specimen

fail but showed signs of damage in the form of small hackles in the adhesive. All specimens that failed during fatigue loading failed due to delamination within the composite.

**Spectrum loading**

The loading on an actual ship structure in extreme wave conditions was determined with the aid of a finite element model. Data was extracted for a critical joint location and used to construct a load histogram for a design life of 25 years using a deterministic approach based on a Weibull distribution of waves[28]. A safety factor of 10 was applied to the number of cycles. This histogram, in terms of equivalent average shear stress (see Figure 10), represents a total of 511 million cycles which is unfeasible for laboratory testing. Based on the S-N curve and applying a safety factor to the fatigue threshold determined above, the histogram is truncated to exclude cycles below 0.5 MPa average shear stress. In order to simplify the histogram, cycle binning over multiple stress ranges was employed, i.e., all cycles within a stress range were accumulated to get the binned number of cycles and the maximum stress level is assigned to the bin. The histogram used for laboratory experiments is also shown in Figure 10. The orange lines represent the number of cycles to be tested in the laboratory for the particular stress level, which is obtained from 'binning' the cycles within the red box. The spectrum loading is primarily developed for fatigue testing of large scale specimens as part of the QUALIFY project[29], the results of which will be presented in future work. Here, the spectrum loading is used to mimic the in-service loads on the double strap joints. The different stress levels applied to the specimen are
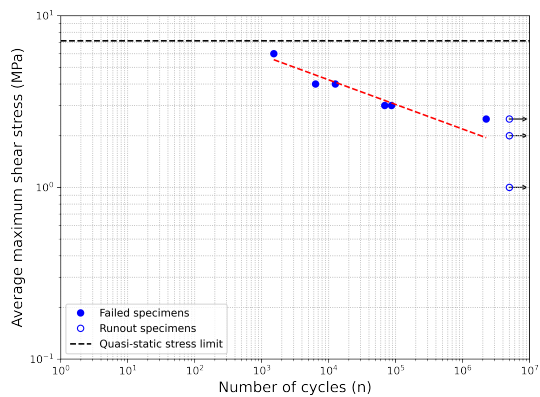
**FIGURE 9** Fatigue data and S-N curve of aged double strap joints

summarised in Table 3.

Specimens 29 and 30 were SF tested for a total of $3.47 \times 10^6$ cycles; both specimens remained intact without any signs of damage. These two specimens were also quasi-statically tested to determine the joint's residual strength after fatigue.
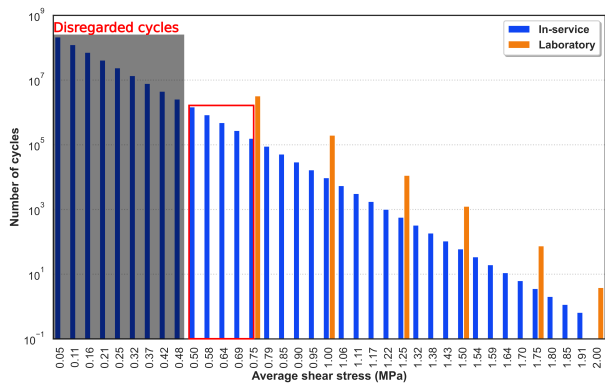


**FIGURE 10** The in-service and laboratory load histograms. The shaded region shows the cycles which are below 0.5 MPa and not further considered for definition of the spectrum loading. The red box represents the binning of cycles above 0.5 MPa stress range. Extracted from QUALIFY project Deliverable 3.3.1

### Residual tensile test

A total of seven specimens were tested quasi-statically until failure to determine the residual strength of the bi-material double strap joint after fatigue loading. Five specimens survived $5 \times 10^6$ cycles under constant amplitude fatigue and two specimens survived $3.47 \times 10^6$ under spectrum loading. An overview of the residual strength of these specimens is given in Table 4; the plot of average shear stress vs average shear strain is shown in Figure 11. Three

**TABLE 3** Summary of spectrum loading

| Block No. | $\tau_{\text{avg}_{\text{max}}}$ | Number of cycles |
|---|---|---|
| 1 | 2.00 MPa | 4 |
| 2 | 1.75 MPa | 76 |
| 3 | 1.50 MPa | 1,265 |
| 4 | 1.25 MPa | 11,420 |
| 5 | 1.00 MPa | 198,830 |
| 6 | 0.75 MPa | 3,265,000 |

The load level equivalent to $\tau_{\text{avg}_{\text{max}}}$ = 0.75 MPa was too low for the servo-hydraulic machine, hence the 1.00 MPa stress level was tested for a total of 3,463,830 cycles instead.

**TABLE 4** Summary of the results from residual tensile tests

(a) CAF tested specimens

| Specimen no. | Max. load | $\tau_{\text{avg}_{\text{max}}}$ | Elongation at failure | $\gamma_{\text{avg}_{\text{max}}}$ |
|---|---|---|---|---|
| 18 | 116.19 kN | 7.75 MPa | 5.33 mm | 33.31% |
| 20 | 106.06 kN | 7.07 MPa | 4.18 mm | 26.13% |
| 21 | 99.80 kN | 6.65 MPa | 4.21 mm | 26.31% |
| 23 | 112.05 kN | 7.47 MPa | 4.74 mm | 29.63% |
| 26 | 104.55 kN | 6.97 MPa | 4.71 mm | 29.44% |

(b) SL tested specimens

| Specimen no. | Max. load | $\tau_{\text{avg}_{\text{max}}}$ | Elongation at failure | $\gamma_{\text{avg}_{\text{max}}}$ |
|---|---|---|---|---|
| 29 | 103.39 kN | 6.89 MPa | 3.40 mm | 21.25% |
| 30 | 120.65 kN | 8.04 MPa | 4.68 mm | 29.25% |

specimens tested under CAF at an average shear stress of 2.5 MPa and 2.0 MPa, showed signs of damage (hackles in the adhesive) at the end of the fatigue tests. However, this damage did not have a significant influence on the joint strength. All specimens failed due to delamination within the composite. The mean residual strength $\tau_{\text{avg}_{\text{max}}}$ is 7.26 MPa with a standard deviation of 0.50 MPa.

Welch's t-test was used to evaluate the (dis)similarity between the shear strength ($\tau_{\text{avg}_{\text{max}}}$) obtained from quasi-static tensile tests and residual tensile strength tests. The hypothesis test $p-\text{value} = 0.3077 > \alpha$ fails to reject the null hypothesis and it can be concluded that there is no significant difference between both.

## 5 | CONCLUSION

Composite to steel double strap joints manufactured in shipyard conditions were subjected to quasi-static tensile testing and various types of fatigue tests. First, a combination of DIC and IRT was used to evaluate the type and evolution of damage in the joints with bondline thickness 4 mm and 8 mm. The specimens exhibited disbond at
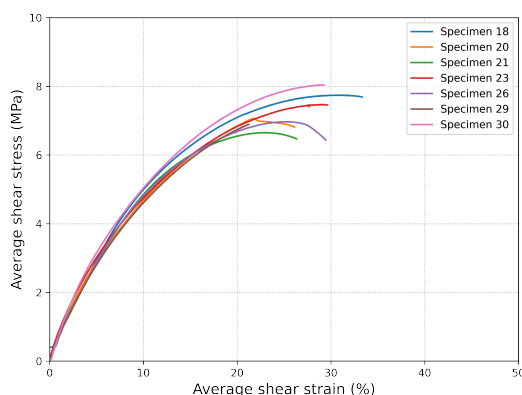
**FIGURE 11** Average shear stress versus average shear strain curve of the residual strength tested specimens

the adhesive-adherend interface along with the formations of hackles in the adhesive. Second, joints with bondline thickness of 8 mm were aged in a salt-spray chamber to determine the S-N curve of the joint and to assess the remaining strength of the joint after fatigue loading. The fatigue tests on the aged specimens showed that all tests at a stress level 1.0 MPa average shear stress led to run-out without damage to the adhesive. Tests at at a stress level 2.00 MPa also led to run-out but small hackles were observed in the adhesive. The S-N curve of the double strap joint can be represented by $N = a \cdot S^{-m}$, with constants $a = 15.81$ and $m = 0.14$. The remaining shear strength of the run-out specimens was statistically not different from the shear strength of the quasi-statically tested specimens that were not fatigue loaded.

## REFERENCES

1. Boyd SW, Blake JIR, Shenoi RA, Kapadia A. Integrity of hybrid steel-to-composite joints for marine application. *Proc. Inst. Mech. Eng. Part M J. Eng. Marit. Environ.* 2004; 218(4): 235–246. http://dx.doi.org/10.1177/147509020421800403 doi: 10.1177/147509020421800403

2. Zuo P, Vassilopoulos AP. Review of fatigue of bulk structural adhesives and thick adhesive joints. *Int. Mater. Rev.* 2020. http://dx.doi.org/10.1080/09506608.2020.1845110 doi: 10.1080/09506608.2020.1845110

3. Broughton W. Testing the mechanical, thermal and chemical properties of adhesives for marine environments. *Adhes. Mar. Eng.* 2012: 99–154. http://dx.doi.org/10.1533/9780857096159.2.99 doi: 10.1533/9780857096159.2.99

4. Harris JA, Fay PA. Fatigue life evaluation of structural adhesives for automative applications. *Int. J. Adhes. Adhes.* 1992; 12(1): 9–18. http://dx.doi.org/10.1016/0143-7496(92)90003-E doi: 10.1016/0143-7496(92)90003-E

5. Banea MD, Silva dLFM. Adhesively bonded joints in composite materials: An overview. *Proc. Inst. Mech. Eng. Part L J. Mater. Des. Appl.* 2009; 223(1): 1–18. http://dx.doi.org/10.1243/14644207JMDA219 doi: 10.1243/14644207JMDA219

6. Tong L. An Assessment of Failure Criteria to Predict the Strength of Adhesively Bonded Composite Double Lap Joints. *J. Reinf. Plast. Compos.* 1997; 16(8): 698–713. http://dx.doi.org/10.1177/073168449701600803 doi: 10.1177/073168449701600803

7. Tsai MY, Morton J. An investigation into the stresses in double-lap adhesive joints with laminated composite adherends. *Int. J. Solids Struct.* 2010; 47(24): 3317–3325. http://dx.doi.org/10.1016/j.ijsolstr.2010.08.011 doi: 10.1016/j.ijsolstr.2010.08.011

8. Silva dLF, Rodrigues TN, Figueiredo MA, Moura dMF, Chousal JA. Effect of adhesive type and thickness on the lap shear strength. *J. Adhes.* 2006; 82(11): 1091–1115. http://dx.doi.org/10.1080/00218460600948511 doi: 10.1080/00218460600948511

9. Crocombe AD. Global yielding as a failure criterion for bonded joints. *Int. J. Adhes. Adhes.* 1989; 9(3): 145–153. http://dx.doi.org/10.1016/0143-7496(89)90110-3 doi: 10.1016/0143-7496(89)90110-3

10. Gleich DM, Van Tooren MJ, Beukers A. Analysis and evaluation of bondline thickness effects on failure load in adhesively bonded structures. *J. Adhes. Sci. Technol.* 2001; 15(9): 1091–1101. http://dx.doi.org/10.1163/156856101317035503 doi: 10.1163/156856101317035503

11. Adams RD, Peppiatt NA. Stress analysis of adhesive-bonded lap joints. *J. Strain Anal.* 1974; 9(3): 185–196. http://dx.doi.org/10.1243/03093247V093185 doi: 10.1243/03093247V093185

12. Saraç Adin H, Temiz Experimental determination of the static and fatigue strength of the adhesive joints bonded by epoxy adhesive including different particles. *Compos. Part B Eng.* 2018; 155: 92–103. http://dx.doi.org/10.1016/J.COMPOSITESB.2018.08.006 doi: 10.1016/J.COMPOSITESB.2018.08.006

13. Broughton WR, Mera RD, Hinopoulos G. Project PAJ3-Combined Cyclic Loading and Hostile Environments Cyclic Fatigue Testing of Adhesive Joints Test Method Assessment. 1996.

14. Nolting AE, Underhill PR, DuQuesnay DL. Variable amplitude fatigue of bonded aluminum joints. *Int. J. Fatigue* 2008; 30(1): 178–187. http://dx.doi.org/10.1016/J.IJFATIGUE.2007.01.027 doi: 10.1016/J.IJFATIGUE.2007.01.027

15. Bernasconi A, Beretta S, Moroni F, Pirondi A. Local Stress Analysis of the Fatigue Behaviour of Adhesively Bonded Thick Composite Laminates. *https://doi.org/10.1080/00218464.2010.484300* 2010; 86(5-6): 480–500. http://dx.doi.org/10.1080/00218464.2010.484300 doi: 10.1080/00218464.2010.484300

16. Zhang Y, Vassilopoulos AP, Keller T. Fracture of adhesively-bonded pultruded GFRP joints under constant amplitude fatigue loading. *Int. J. Fatigue* 2010; 32(7): 979–987. http://dx.doi.org/10.1016/J.IJFATIGUE.2009.11.004 doi: 10.1016/J.IJFATIGUE.2009.11.004

17. Sarfaraz R, Vassilopoulos AP, Keller T. Experimental investigation of the fatigue behavior of adhesively-bonded pultruded GFRP joints under different load ratios. *Int. J. Fatigue* 2011; 33(11): 1451–1460. http://dx.doi.org/10.1016/J.IJFATIGUE.2011.05.012 doi: 10.1016/J.IJFATIGUE.2011.05.012

18. Sarfaraz R, Vassilopoulos AP, Keller T. Experimental investigation and modeling of mean load effect on fatigue behavior of adhesively-bonded pultruded GFRP joints. *Int. J. Fatigue* 2012; 44: 245–252. http://dx.doi.org/10.1016/J.IJFATIGUE.2012.04.021 doi: 10.1016/J.IJFATIGUE.2012.04.021

19. LIU HB, ZHAO XL, AL-MAHAIDI R. EFFECT OF FATIGUE LOADING ON BOND STRENGTH BETWEEN CFRP SHEETS AND STEEL PLATES. *http://dx.doi.org/10.1142/S0219455410003348* 2012; 10(1): 1–20. http://dx.doi.org/10.1142/S0219455410003348 doi: 10.1142/S0219455410003348

20. Wu C, Zhao XL, Chiu WK, Al-Mahaidi R, Duan WH. Effect of fatigue loading on the bond behaviour between UHM CFRP plates and steel plates. *Compos. Part B Eng.* 2013; 50: 344–353. http://dx.doi.org/10.1016/J.COMPOSITESB.2013.02.040 doi: 10.1016/J.COMPOSITESB.2013.02.040

21. Yu QQ, Gao RX, Gu XL, Zhao XL, Chen T. Bond behavior of CFRP-steel double-lap joints exposed to marine atmosphere and fatigue loading. *Eng. Struct.* 2018; 175: 76–85. http://dx.doi.org/10.1016/J.ENGSTRUCT.2018.08.012 doi: 10.1016/J.ENGSTRUCT.2018.08.012

22. Jimenez-Vicaria JD, G. Pulido MD, Castro-Fresno D. Influence of carbon fibre stiffness and adhesive ductility on CFRP-steel adhesive joints with short bond lengths. *Constr. Build. Mater.* 2020; 260: 119758. http://dx.doi.org/10.1016/J.CONBUILDMAT.2020.119758 doi: 10.1016/J.CONBUILDMAT.2020.119758

23. Borrie D, Liu HB, Zhao XL, Singh Raman RK, Bai Y. Bond durability of fatigued CFRP-steel double-lap joints pre-exposed to marine environment. *Compos. Struct.* 2015; 131: 799–809. http://dx.doi.org/10.1016/J.COMPSTRUCT.2015.06.021 doi: 10.1016/J.COMPSTRUCT.2015.06.021

24. ASTM B117 - 11 Standard Practice for Operating Salt Spray (Fog) Apparatus. .

25. Society IDIC, Jones E, Iadicola M. A Good Practices Guide for Digital Image Correlation. tech. rep., International Digital Image Correlation Society; 2018

26. Maxwell D, Mcgregor A. Assessing adhesive bond failures: Mixed-mode bond failures Explained. *J. Chem. Inf. Model.* 2013; 53(9): 1689–1699.

27. Al-Shawaf A, Zhao XL. Adhesive rheology impact on wet lay-up CFRP/steel joints' behaviour under infrastructural sub-zero exposures. *Compos. Part B Eng.* 2013; 47: 207–219. http://dx.doi.org/10.1016/j.compositesb.2012.11.012 doi: 10.1016/j.compositesb.2012.11.012

28. Mouton L, Paboeuf S, Verhaeghe C. COMPOSITE SUPERSTRUCTURE BONDED TO A NAVY SHIP STEEL HULL : CHARACTERISATION OF THE WAVE LOADS APPLIED ON THE JOINT. In: ; 2019; Nantes, France: 503–514.

29. Enabling Qualification of Hybrid Structures for Lightweight and Safe Maritime Transport | 2 Mers Seas Zeeën. .